

Distinguishing Signatures of top-and bottom-type heavy vectorlike quarks at the LHC

Aarti Girdhar ¹

Department of Physics, Dr. B. R. National Institute of Technology, Jalandhar, India
and Regional Centre for Accelerator-based Particle Physics,
Harish-Chandra Research Institute, Chatnaag Road
Jhansi, Allahabad 211019, India

Biswarup Mukhopadhyaya ²

Regional Centre for Accelerator-based Particle Physics, Harish-Chandra Research Institute,
Chatnaag Road, Jhansi, Allahabad 211019, India

Monalisa Patra ³

Department of Theoretical Physics,
Tata Institute of Fundamental Research, Mumbai 400 005, India

Abstract

An $SU(2)$ vectorlike singlet quark with a charge either $+2/3$ (t') or $-1/3$ (b') is predicted in many extensions of the Standard Model. The mixing of these quarks with the top or bottom lead to Flavor Changing Yukawa Interactions and Neutral Current. The decay modes of the heavier mass eigenstates are therefore different from the Standard Model type chiral quarks. The Large Hadron Collider (LHC) will provide an ideal environment to look for the signals of these exotic quarks. Considering all decays, including those involving Z - and Yukawa interactions, we show how one can distinguish between t' and b' from ratios of event rates with different lepton multiplicities. The ability to reconstruct the Higgs boson with a mass around 125.5 GeV plays an important role in such differentiation.

1 Introduction

The Standard Model (SM) of particle physics has enjoyed a remarkable success in explaining various experimental data. Occasionally some observations have shown deviations from the SM expectation, but have disappeared later with the increase in statistics. Nonetheless, the possibility of new physics being indicated by experimental data [1, 2] has constantly driven physicists towards an inspired quest. On the theoretical front, the SM does have some shortcomings as it has too many free parameters and offers no answer to some of the fundamental questions. An example is the issue of naturalness, or the stability of the Higgs boson mass against quadratically divergent corrections. In order to address questions such as this, many theoretical scenarios are exploited, with or without direct connections with the questions asked.

¹Electronic address: aarti@hri.res.in

²Electronic address: biswarup@hri.res.in

³Electronic address: monalisa@theory.tifr.res.in

The currently running Large Hadron Collider (LHC) at CERN (and the next generation accelerators) will hopefully provide us with some clues.

An observation that once created some stir was the measurement of the forward-backward asymmetry (A_b^{FB}) of the b quark [1], by the LEP experiments. It showed about 2.9σ deviation from the value predicted by the best fit to the precision electroweak observables within the SM [3]. In the leptonic sector no such discrepancy was observed. These results have motivated many theories, which resolve this disagreement through the introduction of new quark degrees of freedom or new possible gauge bosons. The study of new quarks mixing with the chiral fermions of the SM has been an important area of investigation for quite some time now. Many theories beyond the SM (BSM) naturally predict the existence of such vectorlike quarks. They have been studied in the context of the superstring-inspired E_6 models [4], Little Higgs theories [5, 6] and also extra dimensional models [7]. Many of these scenarios also predict vectorlike leptons. Our focus, however, will be on vectorlike quarks, since they can be expected to be produced at the LHC through strong interactions. Depending on the context, these vectorlike quarks can exist as triplets, doublets or singlets under $SU(2)_L$ gauge group and can have different hypercharges under $U(1)_Y$. On the other hand the presence of new chiral fermions, like the one predicted by fourth generation theories, with couplings similar to the SM ones, are disfavoured by data [8] which allow a narrow mass window for their survival. The limits on these quarks from various experiments are discussed later.

In a general context, vectorlike quarks can be both top-like (charge $+2/3$) and bottom-like (charge $-1/3$) vector singlet. We consider vectorlike isosinglet quarks in both the sectors as possibilities, taking one at a time in addition to the three generations of SM chiral fermions. The extension of the SM through the inclusion of a weak isospin singlet fermion leads to mixing between the singlet fermions and the SM doublets and hence different phenomenological consequences from what are predicted by the SM. The aim of our work is to distinguish between the singlets top- and bottom-type (t' and b') from their decays. In particular we wish to utilise the fact that the decay into Higgs is possible, and that the mass of the Higgs is known to us now. The dominant decays of t' and b' are expected to be

1. $t' \rightarrow W^+b, \quad t' \rightarrow Ht, \quad t' \rightarrow Zt.$
2. $b' \rightarrow W^-t, \quad b' \rightarrow Hb, \quad b' \rightarrow Zb.$

With the discovery of a Higgs like boson by the LHC experiments [9, 10], the decay mode $t'/b' \rightarrow Ht/b$ is a channel of interest. We make use of this fact and tag five b 's along with the requirement of two b pairs giving invariant mass peaks at m_H for both the isosinglets. We find that we can distinguish between the signals present on account of t' and b' .

The collider phenomenology of these vectorlike isosinglets has been considered extensively in the literature (for most recent ones [11] - [22]). In the earlier works, events are mainly selected with a final state composed of W or Z bosons and jets consistent with the decay of the heavy quarks. Once a signal is obtained, it becomes necessary to pinpoint the new physics scenario which leads to it. Since both t' and b' mimic the same signal through these channels, we are addressing this question by our analysis through the Higgs decay channel.

The outline of the paper is as follows. In section 2 we discuss the couplings of the t' and b' separately to the SM fields, through the effective Lagrangian in a model-independent way. In section 3 we discuss the signal and the background along with the methodology adopted for

the analysis of the signal. In section 4 the results of our numerical analysis based on Monte Carlo simulations is presented. We summarise and conclude in section 5.

2 Phenomenology of t' and b'

Strong processes can produce both t' and b' -type quarks at the LHC with identical rates, through gluon fusion or quark-antiquark annihilation. Such pair-production, whose rates are independent of the degree of singlet-doublet mixing, are the modes relevant for our study. Though single-production is also possible, perhaps with less phase space suppression, it is

- (a) driven by electroweak couplings, and
- (b) suppressed by the singlet-doublet mixing angle(s).

The left and right handed component of the vectorlike quarks have the same quantum number under $SU(3) \times SU(2)_L \times U(1)_Y$ unlike the SM ones which are chiral.

I) $t'_L, t'_R = (3, 1, 4/3)$ with electric charge $+2/3$, and mixes with t .

II) $b'_L, b'_R = (3, 1, -2/3)$ with electric charge $-1/3$, and mixes with b .

2.1 Mixing and Coupling of t' and b'

With the addition of the isosinglet quarks to the SM content, we assume mixing to take place mainly with the third generation of the quarks. We show below the general scheme of mixing in the down sector; the pattern is similar in the up-sector as well. The weak eigenstates are denoted by (d_w, s_w, b_w, b'_w) and they are related to the mass eigenstate by [23, 24]

$$\begin{pmatrix} d_w \\ s_w \\ b_w \\ b'_w \end{pmatrix} = U \begin{pmatrix} d \\ s \\ b \\ b' \end{pmatrix}, \quad (2.1)$$

where

$$U_{4 \times 4} = \begin{pmatrix} V_{3 \times 4} \\ X_{1 \times 4} \end{pmatrix} = \begin{pmatrix} V_{ud} & V_{us} & V_{ub} & V_{ub'} \\ V_{cd} & V_{cs} & V_{cb} & V_{cb'} \\ V_{td} & V_{ts} & V_{tb} & V_{tb'} \\ X_{4d} & X_{4s} & X_{4b} & X_{4b'} \end{pmatrix}. \quad (2.2)$$

The unprimed fields denote the basis, where, the mass matrix of the up-type quarks are diagonalized. The submatrix $V_{3 \times 4}$ consisting of the first three rows of the $U_{4 \times 4}$ matrix is the charged current matrix analogous to the SM CKM matrix and is not unitary. The addition of the fourth row restores the unitarity of U . The charged current interaction in the mass basis is now given by:

$$\mathcal{L}_{CC} = \frac{e}{2\sqrt{2}\sin\theta_W} [\bar{u}_L^i \gamma^\mu V_{ij} d_L^j] W_\mu^+ + h.c. \quad (2.3)$$

where e is the electromagnetic coupling constant, θ_W is the weak mixing angle and V_{ij} is the relevant 3×4 submatrix of U . The indices i, j run over the quark generations ($i = 1-3$, $j =$

1-4), and $u = (u, c, t)$, $d = (d, s, b, b')$. As a consequence of mixing between fields with different weak isospin (T_3), Flavor Changing Neutral Current (FCNC) processes appear at the tree level, something that is absent in the SM framework. We therefore get $b'bZ$ and $b'bH$ interactions. In addition, the $SU(2)$ singlet field b' in the flavor terms can have a gauge invariant 'bare' mass term, contrary to d, s and b . As a result the mass and Yukawa coupling matrices cannot be simultaneously diagonalised, and the physical states can have flavor changing Yukawa interactions. The neutral current interaction in the mass basis is given by:

$$\mathcal{L}_{NC} = \frac{e}{2 \sin 2\theta_W} [\bar{u}_L^k \gamma^\mu u_{kL} - \bar{d}_L^i \gamma^\mu (V^\dagger V)_{ij} d_L^j - 2 \sin^2 \theta_W J_{em}^\mu] Z_\mu \quad (2.4)$$

The index k runs from 1 to 3, whereas i and j runs from 1 to 4. The electromagnetic current J_{em}^μ is diagonal in the mass basis and is

$$J_{em}^\mu = \frac{2}{3} \bar{u}^k \gamma^\mu u_k - \frac{1}{3} \bar{d}^i \gamma^\mu d_i \quad (2.5)$$

The FCNC coupling as seen from Eq. (2.4) is controlled by $V^\dagger V$, which is a 4×4 matrix. Since the mixing matrix $V_{3 \times 4}$ is embedded within the unitary matrix, therefore from Eqs. (2.1), (2.2) we obtain the relation,

$$(V^\dagger V)_{ij} = \delta_{ij} - U_{i4}^* U_{j4}. \quad (2.6)$$

Now let us come to the full explanation of flavor changing Yukawa couplings, already mentioned above. There are gauge invariant mass terms proportional to $\bar{b}'_L b'_R$ and $\bar{b}'_L f'_R$, in the Yukawa coupling sector where $f' = (d, s, b)$, due to non chiral nature of vector quarks. As these terms do not arise from the Yukawa coupling, therefore, the Yukawa matrix cannot be simultaneously diagonalized with the mass matrix through a biunitary transformation, consequently giving rise to non diagonal Yukawa coupling among the physical quarks. The relations go analogously for the top sector. The explicit forms of the Yukawa couplings along with the coupling of the gauge bosons to the vector quarks and SM quarks due to mixing are given as

$$\begin{aligned} \mathcal{L}_{f\bar{f}H} &= \frac{e}{2m_W \sin \theta_W} m_f H \bar{f} (1 - |U_{43}|^2) f \\ \mathcal{L}_{F\bar{F}H} &= \frac{e}{2m_W \sin \theta_W} m_F H \bar{F} (1 - |U_{44}|^2) F \\ \mathcal{L}_{fFH} &= \frac{e}{4m_W \sin \theta_W} H \bar{F} (U_{43}^* U_{44} (m_f (1 + \gamma_5) + m_F (1 - \gamma_5))) f + h.c. \\ \mathcal{L}_{f\bar{f}Z} &= \frac{e\gamma_\mu}{6 \sin 2\theta_W} \bar{f} (3(1 - \gamma_5) |U_{33}|^2 - 4 \sin^2 \theta^W (|U_{33}|^2 + |U_{43}|^2)) f Z^\mu \\ \mathcal{L}_{F\bar{F}Z} &= \frac{e\gamma_\mu}{6 \sin 2\theta_W} \bar{F} (3(1 - \gamma_5) |U_{34}|^2 - 4 \sin^2 \theta^W (|U_{34}|^2 + |U_{44}|^2)) F Z^\mu \\ \mathcal{L}_{fFZ} &= \frac{e\gamma_\mu}{6 \sin 2\theta_W} \bar{f} (3(1 - \gamma_5) (U_{33}^* U_{34}) - 4 \sin^2 \theta_W (U_{33}^* U_{34} + U_{43}^* U_{44})) F Z^\mu + h.c. \\ \mathcal{L}_{f'\bar{F}W} &= \frac{e}{2\sqrt{2} \sin \theta_W} U_{34} \bar{f}' \gamma_\mu (1 - \gamma_5) F W^\mu \\ \mathcal{L}_{FFG} &= g_s \gamma_\mu \bar{F} F G^\mu \end{aligned} \quad (2.7)$$

where f and F are dominantly $SU(2)_L$ doublet and singlet respectively, both in the up and down sectors, and generically stand for mass eigenstates. Moreover, f here denotes third generation quarks only. The CKM matrix elements of the SM involving the light quarks are directly determined from the experiments and are therefore tightly constrained. These

experimental results also give unitary limits on the other elements which cannot be directly determined. The non-observation of the FCNC decays in the top sector by the Tevatron [25] and the analysis of single top production in LEP [26] has set bounds on the CKM matrix elements involving the top quark at 95% CL. A detailed analysis on the allowed mass range and mixing angle θ in accordance with the precision electroweak data, flavor physics and oblique parameters is presented in [27]. They have presented the range of the CKM matrix elements allowed for different quark masses in case of different scenarios. For our analysis we have assumed a simplified version of the matrix given in Eqs. (2.1) and (2.2) and describe all the interactions on the addition of an isosinglet fermion by the following mixing matrix

$$U = \begin{pmatrix} V_{ud} & V_{us} & V_{ub} & 0 \\ V_{cd} & V_{cs} & V_{cb} & 0 \\ V_{td} & V_{ts} & \cos \theta & \sin \theta \\ 0 & 0 & -\sin \theta & \cos \theta \end{pmatrix}. \quad (2.8)$$

We are considering here the mixing of the vector quark with the third generation only as the effect of mixing is very small in the lighter generations for massive vector quarks. The other elements of the mixing matrix are fixed to the SM value. Thus we are essentially considering the isosinglet quark in either sector mixing with the third family alone, the mixing angle being consistent with all existing constraints.

The current phenomenological constraints on vectorlike quarks come from direct production bounds at the various colliders and from flavor physics. There are various direct limits on their masses depending on the decay channel analysed. The CDF collaboration has excluded a heavy t' with SM like couplings at 95% CL up to 358 GeV [28] and a heavy b' with SM like couplings at 95% CL up to 372 GeV [29]. The search mode in the collider experiments is mainly through the pair production of these exotic quarks and further assuming these quarks to only decay through a particular channel. The bound obtained by CDF on b' was by looking for pair produced heavy quark with a 100% branching ratio to $W + \text{SM quarks}$. This analysis mainly constrains all the models predicting this final state. Recent LHC bounds from the ATLAS [30]-[34] and CMS [35] data, have set a lower limit on charge 2/3 and -1/3 exotic quark mass, by the investigation through either a particular decay channel or assuming branching ratios to W , Z and H decay modes in the context of different models. The exclusion of mass of the vectorlike quarks is mainly dependent on the strength of their couplings.

All the possible decay modes of the heavy quarks are considered in our analysis. Flavor constraints are also significant for vectorlike quarks. The mixing of the new quark with the SM quarks leads to the non-unitarity of the 3×3 SM CKM matrix and non-unitarity of this form is tightly constrained as the unitarity triangle of the SM is being measured with absolute precision. The presence of FCNC in this case contributes to some processes such as $b \rightarrow s\gamma$, where the quark b changes its flavor by emitting or absorbing Z or Higgs boson. Along with it a photon is also emitted. The FCNC also leads to b meson mixing such as $B_d - \bar{B}_d$ and $B_s - \bar{B}_s$ mixing [27, 36]. There being enormous activity in the flavor sector, it is expected that the experimental data from this sector can be applied to find constraints on the heavy quarks and their mixing with the SM ones. The constraints obtained in this case are largely model dependent [37, 38] and we do not consider them for our analysis. The benchmark points that we consider for our calculation are presented in Table 1. We present in Fig. 1 the cross section of the vectorlike quark pair production at the 14 TeV LHC. The main production channels are gluon-gluon fusion and $q\bar{q}$ annihilation. The production cross section decreases with the mass

Parameter	Value
$m_{t'}$	350, 500
$m_{b'}$	350, 500
θ	5, 10, 15

Table 1: The various benchmark points used for our analysis, with θ as the mixing angle denoting the $t - t'$ or $b - b'$ mixing.

of the vector quarks and is independent of the mixing angle θ . Moreover the cross section is the same for the two cases considered here. We next show in Fig. 2 the branching ratios of the various decay modes of the vector quarks in the two cases plotted as a function of their mass. We have kept the Higgs mass fixed at $m_H = 125.5$ GeV. These branching ratios are sensitive to the Higgs mass, and have very weak dependence on θ . We have therefore, shown our results for a fixed value of θ .

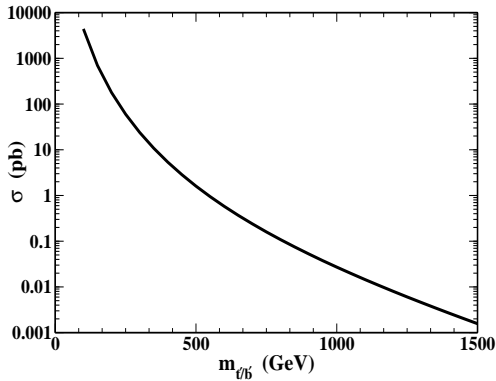


Figure 1: The pair production cross section of t' and b' as a function of mass for mixing angle $\theta = 5$ in a 14 TeV LHC.

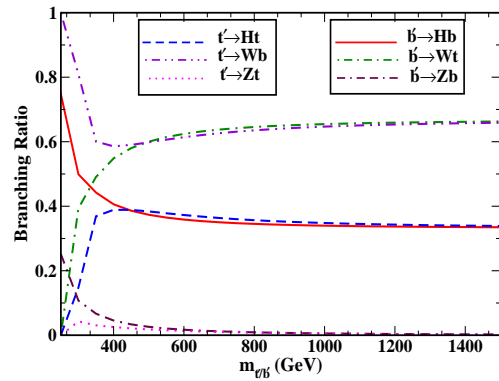


Figure 2: The branching ratios for the vectorlike quarks t' and b' as a function of mass for a fixed mixing angle $\theta = 5$.

3 Signal and Backgrounds

We consider, as already mentioned, the pair production of both $t'\bar{t}'$ and $b'\bar{b}'$, taking one at a time via quark-antiquark as well as gluon pair annihilation.

Signals

With the recent discovery of the Higgs with a mass around 125–126 GeV, we get an added edge, given the fact that the Higgs dominantly decays to $b\bar{b}$ in this mass range. With appropriate tagging, it should be possible to reconstruct the Higgs from the invariant mass of the b -jet pairs. Also, for the allowed range of the mixing matrix elements the branching fractions of t' or b' to Higgs is substantial for moderate masses.

3.1 Signal for t'

We will be mainly concentrating on the decay mode of t' to Higgs and a top quark.

$$pp \rightarrow t'\bar{t}' \rightarrow HtH\bar{t} \rightarrow b\bar{b}W^+bb\bar{b}W^-\bar{b}$$

In this case there can be three possible outcomes depending on the decay mode of both the W 's. It can be either both the W 's are decaying to leptons or one of them is decaying leptonically and the other decaying hadronically, the third possibility is the hadronic decay for both the W 's. Thus the final states arising from $t'\bar{t}'$ production are

- a) $6b + 2l + p'_T$ (leptonic)
- b) $6b + 1l + p'_T + 2 \text{ jets}$ (semileptonic)
- c) $6b + 4 \text{ jets}$ (hadronic),

The same final states can also be obtained from other decay modes of t' . The processes which mimic the $t'\bar{t}'$ decay channel considered for our analysis are

- a) $pp \rightarrow t'\bar{t}' \rightarrow ZtZ\bar{t} \rightarrow b\bar{b}W^+bb\bar{b}W^-\bar{b}$
- b) $pp \rightarrow t'\bar{t}' \rightarrow ZtH\bar{t}/HtZ\bar{t} \rightarrow b\bar{b}W^+bb\bar{b}W^-\bar{b}$

The contribution from these decay channels is proportional to the branching ratio of $Z \rightarrow b\bar{b}$, which is about 15% and too small. It must be remarked that added to the small branching ratio their contribution to the signal gets filtered by the various cuts and the calculation of Higgs invariant mass as explained later.

3.2 Signal for b'

Similar to t' , in this case also we will mainly concentrate on the decay mode of b' to Higgs and bottom quark with the final state consisting of only $6b$'s.

$$pp \rightarrow b'\bar{b}' \rightarrow HbH\bar{b} \rightarrow b\bar{b}b\bar{b}b\bar{b}$$

There are other modes for b' which can give rise to the final state of $6b$'s. Of course, the contributions from all these processes are proportional to the respective branching fractions of $Z \rightarrow b\bar{b}$.

- a) $pp \rightarrow b'\bar{b}' \rightarrow ZbZ\bar{b} \rightarrow b\bar{b}b\bar{b}b\bar{b}$
- b) $pp \rightarrow b'\bar{b}' \rightarrow ZbH\bar{b}/HbZ\bar{b} \rightarrow b\bar{b}b\bar{b}b\bar{b}$

The hadronic decay mode of the W 's from t' will give the same final state signature as b' , provided the jets emitted from the W 's are light. For both t' and b' , we look for the following final state signals, mainly with 5 tagged b 's reconstructing two Higgs in the mass range, 123–128 GeV.

Signal 1: $5b + 2l + p'_T$

Signal 2: $5b + 1l + p'_T$

Signal 3: $5b$

The package CalcHEP v2.5.6 [39] is used to calculate the cross section for the signal process and the respective branching ratios of t' and b' .

Backgrounds

There are many SM processes which can fake the signals listed above. The dominant backgrounds arise from

1. $pp \rightarrow t\bar{t}HH$
2. $pp \rightarrow t\bar{t}H + 2 \text{ jets}$
3. $pp \rightarrow t\bar{t} + N \text{ jets}$, where $0 \leq N \leq 4$
4. $pp \rightarrow t\bar{t}b\bar{b} + N \text{ jets}$, where $0 \leq N \leq 2$
5. $pp \rightarrow W^+W^-HH + N \text{ jets}$, where $0 \leq N \leq 2$

We have computed the cross section for all the background processes except the process $pp \rightarrow t\bar{t}HH$, with ALPGEN [40] which takes into account all the spin correlation and finite width effects. The cross section for the production of $t\bar{t}HH$ is computed with CalcHEP v2.5.6 [39], and is found to be about 0.0005 pb at 14 TeV, for the Higgs mass of 125.5 GeV. Since it is too small to be a threat to our signal, we are not considering this process further in our analysis. A similar argument follows for the background process W^+W^-HH production in association with jets. The cross section is of the order of 10^{-5} pb. Therefore we are also ignoring this process in the further analysis of the background. The QCD factorisation and renormalisation scale (Q^2) in ALPGEN for the different background processes are presented in Table 2.

Process	Q^2
$pp \rightarrow t\bar{t}H$	$(2m_t + 2m_H)^2$
$pp \rightarrow t\bar{t}$	m_t^2
$pp \rightarrow t\bar{t}b\bar{b}$	m_t^2
$pp \rightarrow W^+W^-HH$	$m_W + m_H$

Table 2: The factorisation and renormalisation scale (Q^2) considered for the different background processes in ALPGEN.

3.3 Event Selection Criteria

For the numerical evaluation of both the signal and the background rates, we have considered the CTEQ6L parton distribution function with $m_t = 172$ GeV, $m_b = 4.8$ GeV, $m_H = 125.5$ GeV and centre-of-mass energy, \sqrt{s} of 14 TeV. The signal events along with their decay branching fractions are generated with the help of CalcHEP v2.5.6 [39]. The renormalisation and factorisation scale used for the calculation of production cross sections is the default scale used in CalcHEP, i.e squared sub process centre-of-mass energy ($m_{ij}^2 = \hat{s} = (p_i + p_j)^2$). These signal events are passed on to PYTHIA-6.4.24 [41] for showering and hadronization along with the help of CalcHEP-PYTHIA interface program [42]. We have taken into account in PYTHIA the initial and final state radiations due to QED and QCD, along with the multiple interactions accounting for pile up. The showering of the SM background events is done by passing on the output of ALPGEN [40] in the form of unweighted events to PYTHIA. ALPGEN performs the matching of the jets produced in the showering routine to the partons obtained from the matrix element calculation using the MLM matching procedure [43]. Jet formation is done

through FastJet 3.0.2 [44] using anti- k_t algorithm, with radius parameter $R = 0.4$. The event selection criteria or the cuts applied are the same for both the signal and the background and are detailed below.

- Identification of Isolated Leptons (cut 1):

1) For the lepton trigger, electron candidates are required to have $p_T^e > 25$ GeV and $|\eta| < 2.47$. Moreover the electron is vetoed if it lies in the region $1.37 < |\eta| < 1.52$ between the barrel and endcap electromagnetic calorimeters. The muons are required to satisfy $p_T^\mu > 25$ GeV and $|\eta| < 2.5$.

2) Since we are interested in leptons coming from the decay of on-shell W 's only, they are further tested for being isolated.

a) The total E_T of stable particles within cone radius $\Delta R = \sqrt{(\Delta\eta)^2 + (\Delta\phi)^2} < 0.2$ of the lepton should be less than 10 GeV.

b) In order to make the lepton and jets well separated, we further apply a lepton jet separation cut, $\Delta R_{lj} \geq 0.4$ on the lepton for all the jets formed with $p_T > 20$ GeV. The jets are formed through FastJet [44], with $R = 0.4$ using the anti- k_t jet algorithm. All the particles other than the leptons with trigger of $p_T > 20$ GeV and $|\eta| < 2.5$ form the input for Fastjet. The jets trigger for this is $p_T > 20$ GeV.

c) To exclude the contribution of the same flavor leptons that might come from the decay of Z boson, the invariant mass M_{ll} of the isolated lepton pairs is calculated and the pair having mass in the window $|M_Z \pm 10|$ GeV is discarded. The events chosen after this are listed as those passing cut 1. For the selection in case of signal with one or two isolated leptons, after the application of cut 1 all the events with one or two isolated leptons survive.

- Missing E_T (\cancel{E}_T) (cut 2) :

For the events with one or two isolated leptons, \cancel{E}_T is calculated by computing the vector sum of the visible p_T^{tot} of all particles, where

$$\begin{aligned}\vec{\cancel{E}}_T &= -\Sigma \vec{p}_T^{tot} \\ p_T^{tot} &= \sqrt{(p_x^{tot})^2 + (p_y^{tot})^2} \\ p_x^{tot} &= p_x^{e^\pm} + p_x^{\mu^\pm} + p_x^{jets} + p_x^{unc} \\ p_y^{tot} &= p_y^{e^\pm} + p_y^{\mu^\pm} + p_y^{jets} + p_y^{unc}.\end{aligned}\tag{3.1}$$

In Eq. (3.1) $p_{x,y}^{unc}$ receives contribution from the unclustered components, which consist of the leptons and hadrons in each event not passing the primary selection criteria for trigger but have $p_T > 0.5$ and $|\eta| < 5.0$. A cut of $\cancel{E}_T > 40$ GeV referred to as cut 2 is applied. All the events which survives cut 1, are subjected to this cut.

- b tagging (cut 3):

The jets with $E_T > 40$ GeV and $|\eta| < 2.5$ are selected as trigger for the identification of b jets. A jet is tagged as b jet if it has a b parton within a cone of $\Delta R < 0.4$ with the jet axis and a tagging efficiency of 60% is incorporated. Events with five or more b 's tagged in this manner are selected and are tabulated as events surviving cut 3.

- Invariant Mass Reconstruction :

For the events with at least 5 tagged b 's (surviving after cut 3), invariant mass m_{bb} of all

possible b -jet pairs are computed and those with m_{bb} in the mass range $123 \text{ GeV} \leq m_H \leq 128 \text{ GeV}$ are considered to be coming from the decay of Higgs. We look for the number of events which have at least one b pair in the given Higgs mass range as $\text{NH} \geq 1$. The number of events with two b pairs within the required Higgs mass range are tabulated under $\text{NH} = 2$.

The cuts mentioned above are mainly motivated to suppress the background and also to discriminate the signal of the t' and b' .

3.4 Smearing

In order to account for detector effects, the momenta of the leptons, jets and the unclustered components obtained from the generator are smeared according to the following prescription :

- For electrons and jets: The electrons with pseudorapidity, $|\eta| < 2.5$ and the jets with $|\eta| < 5$ and $p_T > 20 \text{ GeV}$ are smeared by Gaussian distribution given by

$$\frac{\sigma(X)}{X} = \frac{a}{\sqrt{X}} \oplus b \oplus \frac{c}{X} \quad (3.2)$$

where $X = E_T$. In case of the electrons

$$(a, b, c) = \begin{pmatrix} (0.030 \text{ GeV}^{1/2}, 0.005, 0.2 \text{ GeV}) & |\eta| < 1.5 \\ (0.055 \text{ GeV}^{1/2}, 0.005, 0.6 \text{ GeV}) & 1.5 < |\eta| < 1.5 \end{pmatrix}, \quad (3.3)$$

whereas for the jets $a = 0.5 \text{ GeV}^{1/2}$, b and $c = 0$.

- For muons: Muons with $|\eta| < 2.5$ are similarly smeared according to

$$\frac{\sigma(p_T)}{p_T} = \begin{pmatrix} a, & p_T < 100 \text{ GeV} \\ a + b \log \frac{p_T}{100 \text{ GeV}}, & p_T > 100 \text{ GeV} \end{pmatrix} \quad (3.4)$$

with

$$(a, b) = \begin{pmatrix} (0.008, 0.037) & |\eta| < 1.5 \\ (0.020, 0.050) & 1.5 < |\eta| < 1.5 \end{pmatrix} \quad (3.5)$$

- For unclustered components: The stable particles with $|\eta| < 5.0$ and $E_T > 0.5 \text{ GeV}$ are smeared as unclustered components, the corresponding Gaussian width being

$$\sigma(E_T) = \alpha \sqrt{\sum_i E_T^{(unc)_i}}, \quad (3.6)$$

with $\alpha \approx 0.55$. In this case the x and y component of E_T^{unc} are smeared independently by the same quantity.

4 Numerical Results

We have briefly discussed in section 3 about the final state signal along with the various cuts applied for our analysis. We present in this section the actual number of events surviving after each cut for a given integrated luminosity of 100 fb^{-1} . The different final states are briefly described below.

- First of all, we consider the number of events with the final state $5b + 2l + \cancel{p}_T$ (signal 1), i.e. 5 tagged b jets with two b jet pair's invariant mass peaking at the Higgs mass (123–128 GeV) along with 2 isolated leptons, which we call N_1 . The number of events, surviving after each cut for this final state, for the considered integrated luminosity is presented in Table 3 for both the signal and the background processes.

We can see from the table that with the choice of our cuts, we are able to discriminate between the signals of the t' and b' vector quarks. From this table we can make following observations.

- At the production level the number of events for both types of signal and one of the background, $t\bar{t}$, is of the same order of magnitude. The other two SM backgrounds, $t\bar{t}H$, $t\bar{t}b\bar{b}$ are smaller but comparable. This continues even after the application of cut 1 and cut 2. In case of $b'\bar{b}'$, this is because the dominant decay mode of b' being W^-t , the final state will consist of $4W$'s and $2b$'s resulting in large number of events satisfying cut 1 and 2. Similarly, the leptons from the $t\bar{t}$ process survives cut 1 and 2 as the tops produced are highly boosted. It is only after the application of cut 3 which requires at least 5 tagged b 's along with a minimum energy of 40 GeV, the background gets washed away.
- After applying cut 3 the discrimination between the two kinds of signals, $t'\bar{t}'$ and $b'\bar{b}'$ starts to show up. Further demand of reconstructing two Higgs from the tagged b 's makes the distinction between two kinds of signal events quite clear.

We can conclude from this table that in the case of $5b + 2l + \cancel{p}_T$ final state after all the cuts, we expect the dominant contribution from top-like vector quark, t' . The trend seems to be same for both the masses.

$m_{t',b'}$ (GeV)	Process	Actual Number of Events with $\mathcal{L} = 100 \text{ fb}^{-1}$					
		At prod.	cut 1	cut 2	cut 3	NH ≥ 1	NH=2
350	$t'\bar{t}'$	1.08×10^6	3.22×10^4	2.37×10^4	179.30	64.80	8.64
	$b'\bar{b}'$	1.08×10^6	3.91×10^4	3.27×10^4	23.72	5.23	0.69
500	$t'\bar{t}'$	1.60×10^5	4.92×10^3	4.05×10^3	74.69	18.67	1.61
	$b'\bar{b}'$	1.61×10^5	8.09×10^3	7.35×10^3	6.12	1.41	0.1
Background	$t\bar{t}H + 2 \text{ jets}$	1.57×10^4	506.09	409.08	0.701	0	0
	$t\bar{t}b\bar{b} + 2 \text{ jets}$	2.74×10^4	526.75	426.55	2.80	0.60	0.06
	$t\bar{t} + 4 \text{ jets}$	1.74×10^6	3.46×10^4	2.80×10^4	0	0	0

Table 3: Actual number of events in case of the Signal and the Background for a $5b + 2l + \cancel{p}_T$ final state which pass various cuts at the 14 TeV LHC.

- We next consider the number of events with at least 5 tagged b 's and 1 isolated lepton i.e. $5b + 1l + \cancel{p}_T$ (signal 2) in the final state, along with the two b jet pair's invariant mass

peaking at the Higgs mass (123–128 GeV), which we call N_2 . We present the results for this final state, in Table 4 for both t' and b' along with the background. The argument in this case for the number of events surviving after each cut is similar to the previous one. The events that survive even after the Higgs invariant mass reconstruction in case of backgrounds is mainly due to the combinatorics. We next show in Figs. 3, 4, 5 and 6,

$m_{t',b'}$ (GeV)	Process	Actual Number of Events with $\mathcal{L} = 100 \text{ fb}^{-1}$					
		At prod.	cut 1	cut 2	cut 3	NH ≥ 1	NH=2
350	$t't'$	1.08×10^6	2.92×10^5	2.81×10^5	2.56×10^3	743.123	151.21
	$b'\bar{b}'$	1.08×10^6	2.41×10^5	1.81×10^5	338.7	74.25	9.15
500	$t't'$	1.60×10^5	4.23×10^4	4.26×10^4	928.963	228.89	33.31
	$b'\bar{b}'$	1.61×10^5	4.19×10^4	3.54×10^4	79.87	18.2	3.53
Background	$t\bar{t}H + 2 \text{ jets}$	1.57×10^4	4.20×10^3	3.3×10^3	17.51	4.55	0
	$t\bar{t}b\bar{b} + 2 \text{ jets}$	2.74×10^4	6.59×10^3	4.75×10^3	39.24	8.37	1.21
	$t\bar{t} + 4 \text{ jets}$	1.78×10^6	4.37×10^5	3.18×10^5	1.18×10^2	23.76	23.76

Table 4: Actual number of events in case of the Signal and the Background for a $5b + l + \cancel{p}_T$ final state which pass various cuts at the 14 TeV LHC.

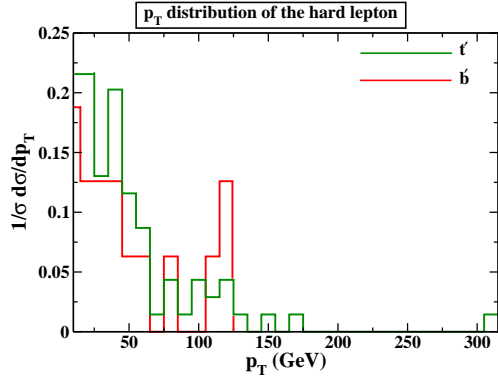


Figure 3: The p_T distribution of the hard lepton after imposing all the cuts for signal 2 for both t' and b' of mass 350 GeV with $\sqrt{s} = 14 \text{ TeV}$.

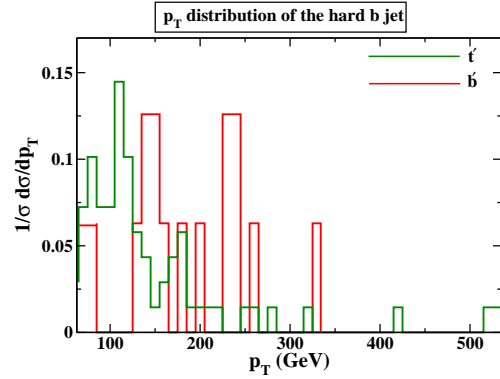


Figure 4: The p_T distribution of hardest b jet after imposing all the cuts for signal 2 for both t' and b' of mass 350 GeV at $\sqrt{s} = 14 \text{ TeV}$.

the different kinematic distributions for this particular signal after all the cuts have been imposed. The p_T distribution of the hard isolated lepton is shown in Fig. 3, whereas Fig. 4 shows the p_T distribution of the hard b jet. Similarly the p_T distribution of the soft b jet is shown in Fig. 5, with Fig. 6 showing the opening angle between the two

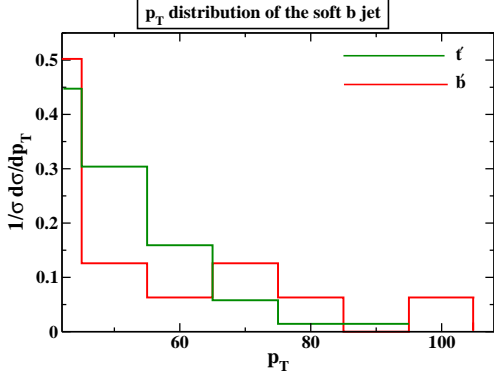


Figure 5: The p_T distribution of the soft b jet after imposing all the cuts for signal 2 for both t' and b' of mass 350 GeV at $\sqrt{s} = 14$ TeV.

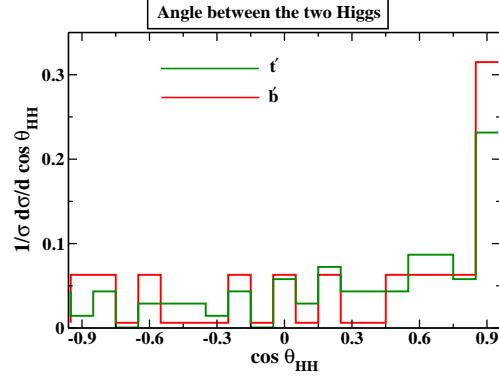


Figure 6: The distribution of opening angle between two reconstructed Higgs after imposing all the cuts for signal 2 for both t' and b' of mass 350 GeV at $\sqrt{s} = 14$ TeV.

reconstructed Higgs. The p_T of the isolated lepton mostly varies between 40–80 GeV, whereas the p_T of the hard b jet varies over a wide range of 80–150 GeV. The p_T of the soft b jet is found to be less than 80 GeV with a peak around 50 GeV. It is seen from the Figures that the distribution pattern of both t' and b' are the same, only with a difference in the statistics. In Figure 6, however, a mild difference is noticed. This is because the lepton final states do not arise in the lowest order in $pp \rightarrow b'\bar{b}' \rightarrow b\bar{b}HH$. The signal is thus the consequence of initial/final states radiation and of cases when it actually arises from $b' \rightarrow tW$, which accidentally mimic two Higgses in an uncorrelated manner.

- Finally the events with at least 5 tagged b jets and zero leptons (signal 3), along with the two b jet pair's invariant mass peaking at the Higgs mass (between 123 GeV and 128 GeV), which we call N_3 , is considered. The result for this is presented in Table 5 for both t' and b' . While considering the zero lepton final state given in Table 5, the cut consisting of isolated lepton and missing energy i.e. cut 1 and 2 is neglected for the obvious reasons. Since both t' and b' favour the hadronic decay mode, it can be seen from the Table, the number of events surviving is the same even after cut 3. It is only after the Higgs mass reconstruction from the b jets, that both t' and b' show different behaviour. Similar to signal 2, we have shown in Figs. 7, 8, 9, 10 the various distributions with all the kinematic cuts imposed. The p_T of the hard b jet is peaked around 200 GeV for $b'\bar{b}'$ pair production, whereas in case of $t'\bar{t}'$, the p_T is peaked around 100 GeV as can be seen from Fig. 7. This is mainly because the b 's from $b'\bar{b}'$ are directly produced from the decay of b' , compared to those from $t'\bar{t}'$, where b is produced from the decay of t' to tH/tZ followed by the decay of t to Wb or H/Z to $b\bar{b}$. The discrimination is reduced when one moves to the p_T distribution of the softer jets, Fig. 8, with both $t'\bar{t}'$ and $b\bar{b}'$ behaving similarly for the p_T distribution of the soft b jet, Fig. 9. The distribution of the opening angle between the two reconstructed Higgs is shown in Fig. 10. The distribution pattern is the same for both t' and b' . It can be seen from the figure that most of the reconstructed Higgs pair have small opening angles, even though the Higgses reconstructed in the signal are also on account of combinatorics. This is because these are real signals, as opposed to the events in Figure 6, and the boost of the parton center-of-mass frame causes a small

opening angle in a large number of cases.

$m_{t',b'}$ (GeV)	Process	Actual Number of Events with $\mathcal{L} = 100 \text{ fb}^{-1}$			
		At prod.	cut 3	NH ≥ 1	NH=2
350	$t't'$	1.08×10^6	1.25×10^4	3.71×10^3	704.26
	$b'\bar{b}'$	1.08×10^6	4.48×10^4	1.11×10^4	1.19×10^3
500	$t't'$	1.60×10^5	3.74×10^3	9.67×10^2	135.25
	$b'\bar{b}'$	1.61×10^5	6.88×10^3	1.23×10^3	110.2
Background	$t\bar{t}H + 2 \text{ jets}$	1.57×10^4	86.51	26.62	3.85
	$t\bar{t}b\bar{b} + 2 \text{ jets}$	2.74×10^4	194.58	42.69	5.78
	$t\bar{t} + 4 \text{ jets}$	1.78×10^6	7.36×10^2	118.78	0

Table 5: Actual number of events surviving after various cuts in case of the Signal and the Background for a $5b$ final state with two b pairs giving an invariant mass peak at the 14 TeV LHC.

From the above analysis, we find a significant difference in the number of events that survive after all the cuts, for both the signals. Still we choose to compute the ratio of the number of events surviving after the application of all cuts in case of the different signals N_i , where $i = 1, 2, 3$ as defined before for both t' and b' . The relevant ratios which we consider are $N_{13} = N_1/N_3$ and $N_{23} = N_2/N_3$ for both t' and b' . We consider these ratios as working with the above rates helps us in getting most of systematic uncertainties cancelled. The results are presented in Table 6 and it can be seen that they differ significantly for t' and b' . We can make

Mass(GeV)	Isosinglet	N_{13}	N_{23}
350	t'	0.012	0.215
	b'	0.0006	0.008
500	t'	0.012	0.246
	b'	0.0009	0.032

Table 6: The ratios, N_{13} and N_{23} for t' and b'

the following observations.

- The ratio N_{13} differs for t' and b' by two orders of magnitude, for both the masses of 350 and 500 GeV.
- The ratio N_{23} differs by a factor of 100 in case of 350 GeV and by a factor of 10 in the case of 500 GeV.

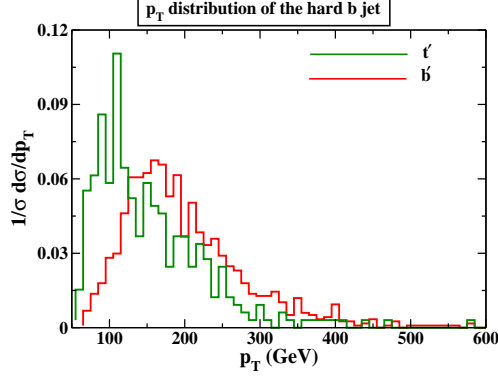


Figure 7: The p_T distribution of the hardest b jet after imposing all the cuts for signal 3 for both t' and b' of mass 350 GeV at $\sqrt{s} = 14$ TeV.

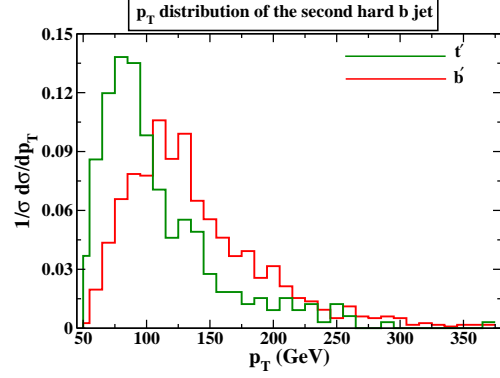


Figure 8: The p_T distribution of second hardest b jet after imposing all the cuts for signal 3 for both t' and b' of mass 350 GeV at $\sqrt{s} = 14$ TeV.

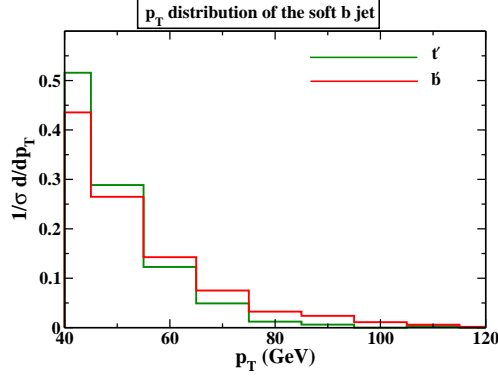


Figure 9: The p_T distribution of the soft b jet after imposing all the cuts for signal 3 for both t' and b' of mass 350 GeV at $\sqrt{s} = 14$ TeV.

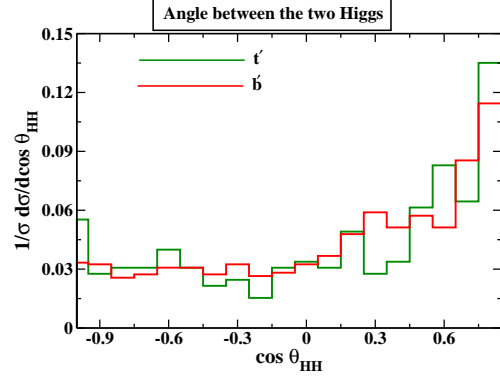


Figure 10: The distribution of opening angle between two reconstructed Higgs after imposing all the cuts for signal 3 for both t' and b' of mass 350 GeV at $\sqrt{s} = 14$ TeV.

It turns out that the ratio N_{13} is a better distinguishing observable than N_{23} and it continues to be so even when the mass of t' , b' increases while N_{23} seems to be sensitive to the t' , b' mass, and can only be used as a distinguishing observable for quarks masses upto 700 GeV.

5 Summary and Conclusions

In this work we have made an attempt to distinguish between top-like and bottom-like isosinglet quarks which are predicted in several extensions of the SM, at a luminosity of 100 fb^{-1} and center-of-mass energy of 14 TeV at the LHC. On account of being vectorlike they mix with third generation chiral quarks which leads to flavor changing Yukawa interactions along with FCNC. These quarks have the decay modes, $t' \rightarrow Zt$, Ht , W^+b and $b' \rightarrow Zb$, Hb , W^-t . We have in this work tried to address the question of distinguishing the signatures of these isosinglet vectorlike quarks once they are discovered.

Choosing in particular the Higgs decay channel out of these possibilities for both t' and b' , we tried to make a distinction between the two cases. The Higgs decays further to a pair of b quarks. We demand that the two Higgs be reconstructed in the mass range 123–128 GeV from the tagged b 's. The recent discovery of Higgs like resonance at 125.5 GeV at the LHC strengthens our analysis. We choose three final states with 2, 1, 0 lepton along with five tagged b 's which is attainable at the LHC as it can efficiently detect leptons and also tag b 's. We find that with a suitable choice of cuts, the SM background is very small for both the signals. Our study overall reveals that, empowered by our recent information on the Higgs, we can clearly differentiate between t' and b' from ratios of events with various lepton multiplicities in the final state along with two reconstructed Higgs.

6 Acknowledgement

AG is thankful to Department of Science and Technology, New Delhi, for funding the work done here through the Women in Science scheme (grant number-(WOS-A/PS-04/2009)). BM acknowledges the funding available from the Department of Atomic Energy, Government of India, for the Regional Centre for Accelerator based Particle Physics(RECAPP), Harish-Chandra Research Institute. MP would like to extend her thanks to RECAPP for the local hospitality and computational assistance during the course of this work.

References

- [1] M. S. Chanowitz, Phys. Rev. Lett. **87**, 231802 (2001) [arXiv:hep-ph/0104024].
- [2] T. Aaltonen *et al.* [CDF Collaboration], Phys. Rev. Lett. **101**, 202001 (2008) [arXiv:0806.2472 [hep-ex]].
- [3] G. Alexander *et al.* [LEP Collaborations and ALEPH Collaboration and DELPHI Collaboration], Phys. Lett. B **276**, 247 (1992).
- [4] V. D. Barger, N. Deshpande, R. J. N. Phillips and K. Whisnant, Phys. Rev. D **33**, 1912 (1986) [Erratum-ibid. D **35**, 1741 (1987)].
- [5] N. Arkani-Hamed, A. G. Cohen, E. Katz, A. E. Nelson, T. Gregoire and J. G. Wacker, JHEP **0208**, 021 (2002) [arXiv:hep-ph/0206020].
- [6] N. Arkani-Hamed, A. G. Cohen, E. Katz and A. E. Nelson, JHEP **0207**, 034 (2002) [arXiv:hep-ph/0206021].
- [7] H. C. Cheng, B. A. Dobrescu and C. T. Hill, arXiv:hep-ph/0004072.
- [8] S. Chatrchyan *et al.* [CMS Collaboration], Phys. Rev. D **86**, 112003 (2012) [arXiv:1209.1062 [hep-ex]].
- [9] [ATLAS Collaboration], Phys. Lett. B **716**, 1 (2012) [arXiv:1207.7214 [hep-ex]].
- [10] [CMS Collaboration], Phys. Lett. B **716**, 30 (2012) [arXiv:1207.7235 [hep-ex]].
- [11] B. Mukhopadhyaya, A. Ray and A. Raychaudhuri, Phys. Lett. B **186**, 147 (1987).

- [12] F. del Aguila, L. Ametller, G. L. Kane and J. Vidal, Nucl. Phys. B **334**, 1 (1990).
- [13] F. del Aguila, J. A. Aguilar-Saavedra and R. Miquel, Phys. Rev. Lett. **82**, 1628 (1999) [arXiv:hep-ph/9808400].
- [14] F. del Aguila and J. A. Aguilar-Saavedra, arXiv:hep-ph/9906461.
- [15] J. A. Aguilar-Saavedra, Phys. Lett. B **625**, 234 (2005) [Erratum-ibid. B **633**, 792 (2006)] [arXiv:hep-ph/0506187].
- [16] J. A. Aguilar-Saavedra, JHEP **0911**, 030 (2009) [arXiv:0907.3155 [hep-ph]].
- [17] B. Bhattacharjee, M. Guchait, S. Raychaudhuri and K. Sridhar, Phys. Rev. D **82**, 055006 (2010) [arXiv:1006.3213 [hep-ph]].
- [18] S. Gopalakrishna, T. Mandal, S. Mitra and R. Tibrewala, Phys. Rev. D **84**, 055001 (2011) [arXiv:1107.4306 [hep-ph]].
- [19] A. Girdhar, Pramana **81** (2013) 975 [arXiv:1204.2885 [hep-ph]].
- [20] L. Wang and X. F. Han, Phys. Rev. D **86**, 095007 (2012) [arXiv:1206.1673 [hep-ph]].
- [21] N. Bonne and G. Moreau, Phys. Lett. B **717**, 409 (2012) [arXiv:1206.3360 [hep-ph]].
- [22] Y. Okada and L. Panizzi, Adv. High Energy Phys. **2013**, 364936 (2013) [arXiv:1207.5607 [hep-ph]].
- [23] B. Mukhopadhyaya and S. Nandi, Phys. Rev. Lett. **66**, 285 (1991).
- [24] B. Mukhopadhyaya and S. Nandi, Phys. Lett. B **266**, 112 (1991).
- [25] F. Abe *et al.* [CDF Collaboration], Phys. Rev. Lett. **80**, 2525 (1998).
- [26] G. Abbiendi *et al.* [OPAL Collaboration], Phys. Lett. B **521**, 181 (2001) [arXiv:hep-ex/0110009].
- [27] J. A. Aguilar-Saavedra, Phys. Rev. D **67**, 035003 (2003) [Erratum-ibid. D **69**, 099901 (2004)] [arXiv:hep-ph/0210112].
- [28] T. Aaltonen *et al.* [CDF Collaboration], Phys. Rev. Lett. **107**, 261801 (2011) [arXiv:1107.3875 [hep-ex]].
- [29] T. Aaltonen *et al.* [CDF Collaboration], Phys. Rev. Lett. **106**, 141803 (2011) [arXiv:1101.5728 [hep-ex]].
- [30] The ATLAS collaboration, ATLAS-CONF-2013-051.
- [31] The ATLAS collaboration, ATLAS-CONF-2013-056.
- [32] The ATLAS collaboration, ATLAS-CONF-2013-060.
- [33] G. Aad *et al.* [ATLAS Collaboration], Phys. Lett. B **718**, 1284 (2013) [arXiv:1210.5468 [hep-ex]].

- [34] G. Aad [ATLAS Collaboration], Phys. Rev. Lett. **108**, 261802 (2012) [arXiv:1202.3076 [hep-ex]].
- [35] S. Chatrchyan [CMS Collaboration], Phys. Rev. Lett. **107**, 271802 (2011) [arXiv:1109.4985 [hep-ex]].
- [36] F. J. Botella, G. C. Branco and M. Nebot, JHEP **1212**, 040 (2012) [arXiv:1207.4440 [hep-ph]].
- [37] M. Aoki, E. Asakawa, M. Nagashima, N. Oshimo and A. Sugamoto, Phys. Lett. B **487**, 321 (2000) [arXiv:hep-ph/0005133].
- [38] M. Aoki, G. C. Cho, M. Nagashima and N. Oshimo, Phys. Rev. D **64**, 117305 (2001) [arXiv:hep-ph/0102165].
- [39] A. Pukhov *et al.*, arXiv:hep-ph/9908288.
- [40] M. L. Mangano, M. Moretti, F. Piccinini, R. Pittau and A. D. Polosa, JHEP **0307**, 001 (2003) [arXiv:hep-ph/0206293].
- [41] T. Sjostrand, S. Mrenna and P. Z. Skands, JHEP **0605**, 026 (2006) [arXiv:hep-ph/0603175].
- [42] A. S. Belyaev, E. E. Boos, A. N. Vologdin, M. N. Dubinin, V. A. Ilyin, A. P. Kryukov, A. E. Pukhov and A. N. Skachkova *et al.*, hep-ph/0101232.
- [43] M. L. Mangano, M. Moretti, F. Piccinini and M. Treccani, JHEP **0701**, 013 (2007) [hep-ph/0611129].
- [44] M. Cacciari, G. P. Salam and G. Soyez, Eur. Phys. J. C **72**, 1896 (2012) [arXiv:1111.6097 [hep-ph]].